APPLICATION OF EPML/TLM TO UWB ANTENNA ANALYSIS

Sebastian Held, Markus Neinhüs and Adalbert Beyer
Department of Electrical Engineering
and Information Sciences
Universität Duisburg-Essen
Duisburg, Germany
email: sebastian.held@uni-due.de

ABSTRACT
Antenna analysis with Transmission Line Matrix (TLM) method requires the use of an absorbing boundary condition in order to simulate a free space environment. This absorbing boundary condition is realized by the EPML (extended perfectly matched layer). This paper demonstrates the capability of this simulation method for practical broadband antenna design. Therefore a bow-tie and vivaldi antenna are analyzed and numerical as well as experimental results are introduced and discussed.

KEY WORDS
Computational Electromagnetics, Antenna measurements, Simulation.

1 Introduction

The validation of new antennas for UWB (ultra wideband) communications can be accomplished using simulation software. In order to get significant results, adequate approximation of free space is required. In practice, the reflection of electromagnetic waves at the boundary should be avoided. One solution to this problem is the TLM method in conjunction with EPML published by Le Maguer [1] in 2001. It offers all the capabilities regularly found in PMLs plus attenuation of evanescent energy. It has proven superior stability in antenna analysis.

Using this particular PML implementation, the spatial distance between the AUT (antenna under test) and the surrounding absorber can be kept very small.

2 Simulation setup

All simulations were done using the SCN developed by Johns [2] with $\Delta_l = \Delta_x = \Delta_y = \Delta_z$. The perfectly matched layer surrounds the computation domain. Its properties beside a geometric profile are:

$$\text{thickness} = 5\Delta_l$$
$$\text{reflection } R_0 = 0.1\%$$
$$\text{evanescent damp. } F = 3$$

The PML is terminated by a matched impedance. The distance between the substrate and the PML layer is $5\Delta_l$.

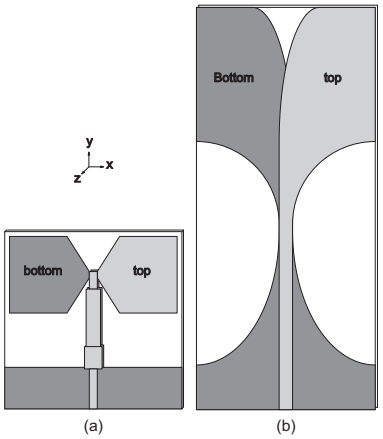

Figure 1. Geometry of the bow-tie (a) and vivaldi (b) antenna.

The excitation is realized by a matched source feeding the microstrip structure. An SMA-connector generally used in measurements is omitted in the simulation. Extraction of scattering parameters is done with help of the algorithm of [3].

3 Antenna simulations

3.1 Bow-Tie antenna

In order to demonstrate the effectiveness of this absorbing boundary condition, we restudy the bow-tie antenna described by Kiminami et al [4]. The published results for the simulated frequency response differ from the measurement, therefore a resimulation was done.

The geometry of the analyzed double-sided printed bow-tie antenna is shown in Fig. 1a. This antenna was fabricated on Duroid substrate with a relative permittivity of 6.15 and a thickness of 1.27 mm. In contrast to the simulation, it is equipped with a SMA-connector in order to fit easily with our HP8722C network analyzer. Thus, the reflection from the coax-microstrip junction is not present in the simulation, but is kept as small as possible.

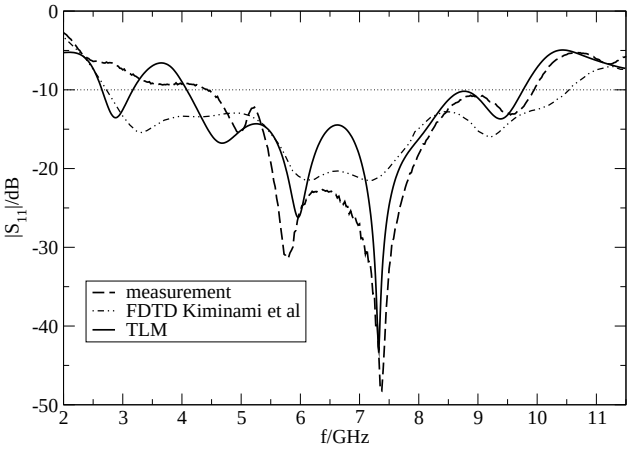

Figure 2. Reflection coefficient $|S_{11}|$ for the bow-tie antenna.

3.2 Vivaldi antenna

The second antenna we investigated, is an antipodal vivaldi antenna [5] (Fig. 1b). It was printed on Duroid 5870 ($\varepsilon_r = 2.33$, thickness 1.575 mm). In contrast to [5], the antenna analyzed in this paper consists of only one substrate. Both were fabricated, but feeding the symmetric vivaldi antenna (constructed out of two substrates glued together) was quite difficult. Hence the physical properties of that antenna differ too much from the intended ones.

4 Simulation results

The simulator is a self written TLM based program with the capability of calculating the reflection coefficient and the far-field radiation pattern in either frequency and time domain [6].

4.1 Bow-tie antenna

The magnitude of the reflection coefficient S_{11} is plotted in Fig. 2. The simulated reflection coefficient reasonably agrees with the measured results. Compared to [4], the resonance at 7.4 GHz is well predicted in the simulation. The antenna is usable between 4.5 GHz - 10 GHz, where the reflection coefficient is below -10 dB. It is a common practice to consider an antenna matched, if the reflection coefficient is smaller than -10 dB.

The azimuthal and elevation patterns are shown in Fig. 3 and Fig. 4, respectively. Since measurements of antenna patterns were not given in [4], only recent measurements and TLM calculations are shown. The differences between measurement and simulation are due to limited performance of our anechoic chamber. The influence of the test fixture is not negligible.

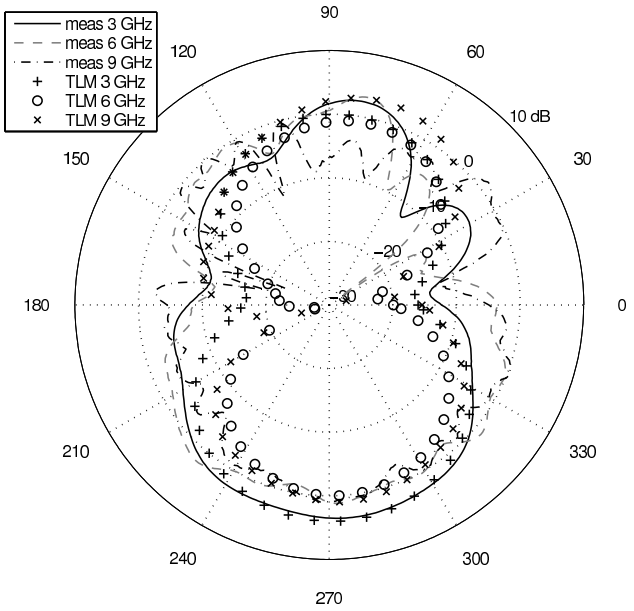

Figure 3. Bow-tie azimuthal radiation patterns.

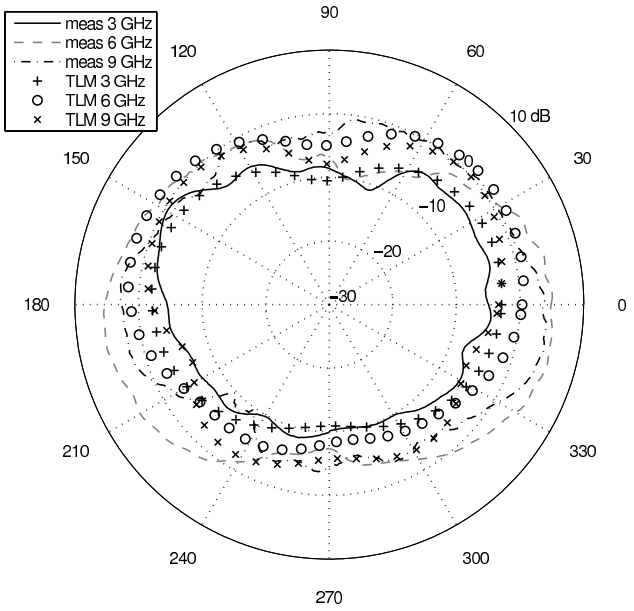

Figure 4. Bow-tie elevation radiation patterns.

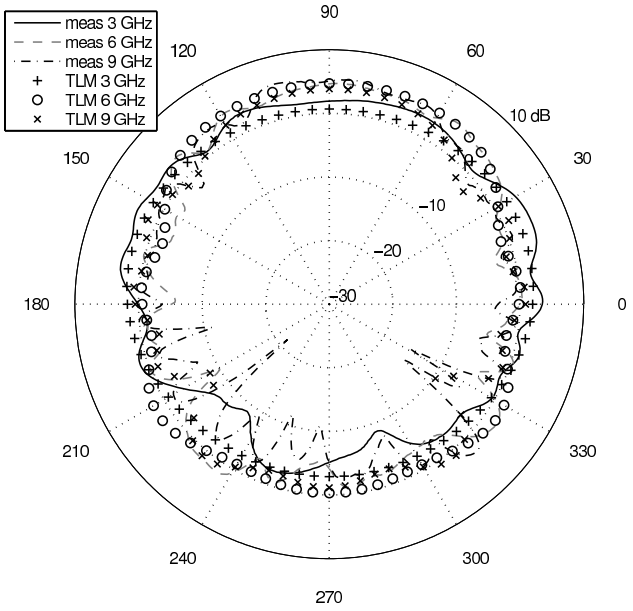

Figure 5. Vivaldi azimuthal radiation patterns.

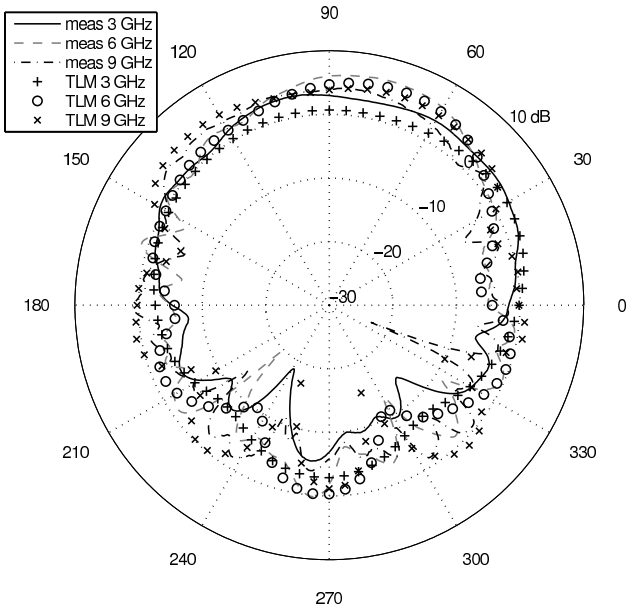

Figure 6. Vivaldi elevation radiation patterns.

4.2 Vivaldi antenna

This type of antenna is particularly useful for broadband transmission, because of its frequency constant omni directional radiation pattern. The azimuthal and elevation patterns are shown in Fig. 5 and Fig. 6.

The simulation accurately predicts the performance of the vivaldi antenna, knowing that the differences around $270°$ arise from our test-fixture.

From Fig. 7 we see that the antipodal vivaldi antenna is not well matched to the $50\,\Omega$-SMA connector of our vector network analyzer. Hence it slightly misses the -10 dB matching line. At this point the antenna shows optimization potential. Similar to the report [5], the simulation does not exactly coincide with the measurement, but follows its characteristic.

Regarding UWB performance, the pulse transmission capability of an antenna is important. Fig. 8 shows a gauss monocycle pulse as excitation signal and the transmitted pulse (θ-polarized e-field) in the farfield ($\phi = 90°, \theta = 90°$). Time and amplitude are normalized (see [7]) for better displaying. The farfield signal exhibits only small disturbances, so called ringing. This antenna is well suited for pulse transmission.

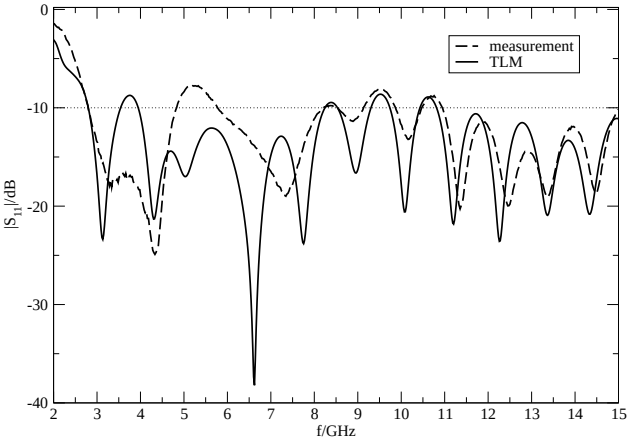

Figure 7. Reflection coefficient $|S_{11}|$ for the vivaldi antenna.

5 Summary

In this paper the capability of EPML in conjunction with the TLM method has been demonstrated by means of a double-sided printed bow-tie antenna and an antipodal vivaldi antenna. Radiation patterns as well as scattering parameters are introduced and discussed. In addition, corrected equations for the SCN-EPML were presented.

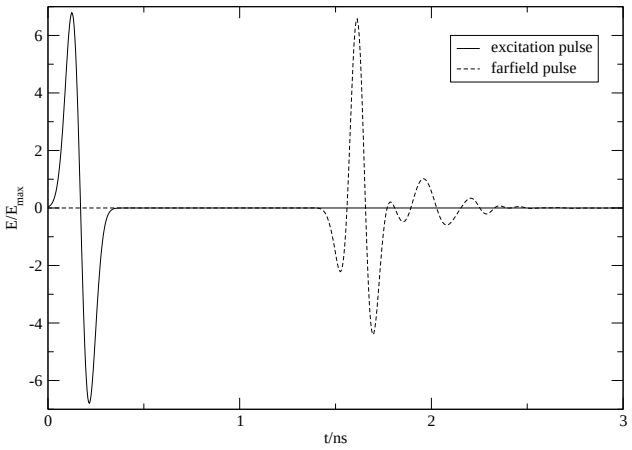

Figure 8. Normalized radiated E-field pulse from the vivaldi antenna.

Appendix

SCN-EPML Equations

In the original publication of Le Maguer [1], there are two errors in the governing equations for EPML using the SCN (symmetrical condensed node). Here are the corrections:

$$\begin{aligned}
\Delta i E_{ij}^{(n)} &= A_{eij}\, C_{ij}\big(a_{jni} + a_{jpi} + Y_{sij}\, a_{eij} - 2a_{eik}\big) \\
\Delta i E_{ik}^{(n)} &= A_{eik}\, C_{ik}\big(a_{kni} + a_{kpi} + Y_{sik}\, a_{eik} - 2a_{eij}\big) \\
Z_0 \Delta i H_{ij}^{(n)} &= A_{mij}\, D_{ij}\big(a_{jnk} - a_{jpk} + Z_{sij}\, a_{mij} \\
&\quad - 2a_{mik}\big) \\
Z_0 \Delta i H_{ik}^{(n)} &= A_{mik}\, D_{ik}\big(- a_{knj} + a_{kpj} + Z_{sik}\, a_{mik} \\
&\quad - 2a_{mij}\big)
\end{aligned}$$

$$\begin{aligned}
C_{ij} &= \frac{c_0 \Delta t \Delta i}{\varepsilon_{ri} \alpha_j \Delta j \Delta k} & D_{ij} &= \frac{c_0 \Delta t \Delta i}{\mu_{ri} \alpha_j \Delta j \Delta k} \\
Y_{sij} &= 4\left(\frac{\varepsilon_{ri} \alpha_j \Delta j \Delta k}{2 c_0 \Delta t \Delta i} - \frac{1}{2}\right) & A_{eij} &= \frac{4}{4 + G_{ij}} \\
Z_{sij} &= 4\left(\frac{\mu_{ri} \alpha_j \Delta j \Delta k}{2 c_0 \Delta t \Delta i} - \frac{1}{2}\right) & A_{mij} &= \frac{4}{4 + R_{ij}} \\
G_{ij} &= Z_0 \frac{2 \sigma_j c_0 \Delta t}{\varepsilon_{ri}} & R_{ij} &= \frac{2 \sigma_j^* c_0 \Delta t}{\mu_{ri} Z_0}
\end{aligned}$$

The explanation of the individual quantities is given in [1].

References

[1] S. Le Maguer and M. M. Ney, Extended PML-TLM node: an efficient approach for full-wave analysis of open structures, *International Journal of Numerical Modeling: Electronic Networks, Devices and Fields*, no. 14, pp. 129-144, 2001.

[2] P. B. Johns, A Symmetrical Condensed Node for the TLM Method, *IEEE Trans., vol. MTT-35*, no. 4, pp. 370-377, April 1987.

[3] Wojciech K. Gwarek and Malgorzata Celuch-Marcysiak, A Differential Method of Reflection Coefficient Extraction From FDTD Simulations, *IEEE Microwave and Guided Wave Letters, vol. 6*, no. 5, May 1996.

[4] Katsuki Kiminami, Akimasa Hirata and Toshiyuki Shiozawa, Double-Sided Printed Bow-Tie Antenna for UWB Communications, *IEEE Antennas and Wireless Propagation Letters, vol. 3*, pp. 152-153, 2004.

[5] "The 2000 CAD Benchmark", *Microwave Engineering Europe*, URL: www.mwee.com.

[6] Allen Taflove and Susan C. Hagness, *Computational Electrodynamics: the finite-difference time-domain method* (Norwood, Artech House, 2000).

[7] Raymond J. Luebbers et al., A Finite-Difference Time-Domain Near Zone to Far Zone Transformation, *IEEE Transactions on Antennas and Propagation, vol. 39*, no. 4, April 1991.